



The influence of diabatic heating in the South Pacific Convergence Zone on Rossby wave propagation and the mean flow

Journal:	<i>QJRMS</i>
Manuscript ID:	QJ-15-0136.R2
Wiley - Manuscript type:	Research Article
Date Submitted by the Author:	06-Sep-2015
Complete List of Authors:	van der Wiel, Karin; University of East Anglia, Centre for Ocean and Atmospheric Sciences Matthews, Adrian; University of East Anglia, School of Environmental Sciences Joshi, Manoj; University of East Anglia, Centre for Ocean and Atmospheric Sciences Stevens, David; University of East Anglia,
Keywords:	SPCZ, diabatic heating, tropical-extratropical interactions, Rossby waves, IGCM4

SCHOLARONE™
Manuscripts

view

The influence of diabatic heating in the South Pacific Convergence Zone on Rossby wave propagation and the mean flow

Karin van der Wiel^{a,b,*}, Adrian J. Matthews^{a,b,c}, Manoj M. Joshi^{a,b,d}, David P. Stevens^{a,c}

^a*Centre for Ocean and Atmospheric Sciences, University of East Anglia, Norwich UK*

^b*School of Environmental Sciences, University of East Anglia, Norwich UK*

^c*School of Mathematics, University of East Anglia, Norwich UK*

^d*Climatic Research Unit, University of East Anglia, Norwich, UK*

*Correspondence to: K. van der Wiel, School of Environmental Sciences, University of East Anglia, Norwich Research Park, Norwich, NR4 7TJ, UK. E-mail: k.van-der-wiel@uea.ac.uk

The South Pacific Convergence Zone (SPCZ) is a northwest-southeast oriented precipitation band over the South Pacific Ocean. Latent heat release from condensation leads to substantial diabatic heating, which has potentially large impacts on local and global climate. The influence of this diabatic heating within the SPCZ is investigated using the Intermediate General Circulation Model (IGCM4).

Precipitation in the SPCZ has been shown to be triggered by transient Rossby waves that originate in the Australian subtropical jet and are refracted towards the equatorial eastern Pacific. A Rossby wave triggers a SPCZ ‘convective event’, with associated diabatic heat release and vortex stretching. Consequently, the Rossby wave is dissipated in the SPCZ region. These features are simulated well in a control integration of IGCM4.

In an experiment, convective heating is prescribed to its ‘climatological’ value in the SPCZ region during the Rossby wave ‘events’ and dynamic forcing from Rossby waves is decoupled from the usual thermodynamic response. In this experiment Rossby waves over the SPCZ region are not dissipated, confirming the vortex stretching mechanism from previous studies. Furthermore, the change in Rossby wave propagation has an impact on momentum transport. Overall, the effect of the Rossby wave-induced convection in the SPCZ is to decrease the strength of the Pacific subtropical jet and the equatorial eastern Pacific upper-tropospheric westerlies, by about 2–6 m s⁻¹.

Following these changes to the basic state, two potential feedbacks in the SPCZ and larger Pacific climate system are suggested: increased SPCZ convection due to the enhancement of negative zonal stretching deformation in the SPCZ region and decreased equatorward refraction of Rossby waves into the westerly duct leading to less SPCZ ‘events’. As the convective events in the SPCZ have a significant impact on Pacific mean climate, it is crucial that the SPCZ is represented correctly in climate models.

Key Words: SPCZ; diabatic heating; tropical-extratropical interaction; Rossby waves

Received ...

1. Introduction

During austral summer, the South Pacific Convergence Zone (SPCZ) is a distinct feature in the distribution of precipitation over the southwestern Pacific Ocean (Figure 1a). It stretches diagonally, northwest-southeast, from New Guinea to about 30°S, 120°W in the central Pacific Ocean (Vincent 1994). Its diagonal orientation is fundamentally different from the zonally oriented Intertropical Convergence Zone (ITCZ) in the northern hemisphere. The SPCZ provides vital precipitation to many Pacific island states. Past changes in its strength or position due to intraseasonal (e.g. the Madden-Julian Oscillation, MJO), interannual (e.g. El Niño-Southern Oscillation, ENSO) or interdecadal (e.g. the Interdecadal Pacific Oscillation, IPO) variability have had significant influences on the region (Griffiths *et al.* 2003; Kumar *et al.* 2006; Vincent *et al.* 2011; Cai *et al.* 2012; Haffke & Magnusdottir 2013; Murphy *et al.* 2014).

The large-scale SPCZ precipitation pattern was first observed when satellite images became available (Hubert 1961; Streten 1973). Since then, many studies have shown that tropical-extratropical interactions by means of transient Rossby waves are related to SPCZ precipitation (e.g. Trenberth 1976; Kiladis & Weickmann 1992, 1997; Matthews *et al.* 1996; Widlansky *et al.* 2011; Matthews 2012; Van der Wiel *et al.* 2015a). Atmospheric processes on intraseasonal and interannual time scales (e.g. MJO, ENSO) set an atmospheric mean state on which synoptic Rossby waves propagate (Meehl *et al.* 2001). Rossby wave propagation is limited to areas where the mean zonal wind field (\bar{u}) is westerly relative to the phase speed of the wave (c), i.e. $\bar{u} - c > 0$. At the boundary $\bar{u} - c = 0$ Rossby waves are evanescent; in areas of mean relative easterly winds ($\bar{u} - c < 0$) there will be no influence by Rossby waves from outside this region. Zonal and meridional asymmetries of the atmospheric mean state direct propagating Rossby waves, e.g. jet streams can act as a wave guide, and the upper-tropospheric westerly winds over the equatorial east Pacific and Atlantic (the ‘westerly ducts’) play an important role in steering waves exiting the jet (Hoskins & Ambrizzi 1993; Ambrizzi *et al.* 1995). Transient Rossby waves are a crucial part of the tropical momentum balance (Kiladis 1998).

Besides tropical-extratropical interactions, other (local) processes have also been suggested to impact the SPCZ. The direct atmospheric impact of land-sea contrasts and orography is minimal (Kiladis *et al.* 1989; Widlansky *et al.* 2011; Van der Wiel *et al.* 2015b). However, the blocking effect of the Andes mountain range enhances subsidence and cools Sea Surface Temperatures (SSTs) locally over the eastern Pacific. Both processes result in an enhancement of the east Pacific dry-zone, which influences the eastern margin of the SPCZ (Takahashi & Battisti 2007a,b; Lintner & Neelin 2008; Niznik & Lintner 2013). Moisture transport and convergence in the lower troposphere are important factors in establishing the SPCZ diagonal orientation (Van der Wiel *et al.* 2015b).

In Matthews (2012) and Van der Wiel *et al.* (2015a) observational-based data products are used to develop a framework to describe a mechanism that forces diagonal bands of convective precipitation in the SPCZ. Rossby waves from the Australian subtropical jet are refracted towards the westerly duct over the equatorial eastern Pacific. In this process, initial circular vorticity centres are elongated and develop a northwest-southeast, diagonal, orientation, caused by advection by the mean flow and Rossby refraction (Hoskins *et al.* 1983; Van der Wiel *et al.* 2015a). Ahead of cyclonic vorticity centres poleward flow enhances ascent in a band parallel to the diagonally oriented cyclone. In the tropical conditionally unstable atmosphere this triggers deep convection. Latent heat release in the convection enhances the ascending motions. The upper-tropospheric divergence associated with the convection and ascent is a source of anticyclonic vorticity through vortex stretching. The propagating cyclonic vorticity centres encounter this anticyclonic tendency; consequently the cyclones are weakened and dissipated in situ.

In this framework, Rossby waves ultimately dissipate themselves by means of a negative feedback involving convection and diabatic heating due to latent heat release from condensation. This is consistent with the observation of Trenberth (1976) that the SPCZ area acts as a ‘graveyard region for fronts moving from the southwest’. This is associated with the deceleration of Rossby waves over the SPCZ area due to negative zonal stretching deformation in the basic state ($\partial U/\partial x < 0$), as discussed by Widlansky *et al.* (2011). Here, we will test the validity of

the proposed framework in an Atmospheric General Circulation Model (AGCM) of intermediate complexity. Furthermore, we will investigate the influence of diabatic heating from convective events in the SPCZ on the regional mean flow. Tropical convection and associated heating is a substantial source of energy, the dynamical responses to this forcing has been the topic of many studies. Theoretically, the Gill-Matsuno model explains the generation and development of an equatorial Kelvin and Rossby wave response to localised tropical heating (e.g. as observed in the MJO, Matsuno 1966; Gill 1980). However, the dynamical response to tropical heating is not limited to the tropics (e.g. Qin & Robinson 1993; Jin & Hoskins 1995; Matthews *et al.* 2004). The explicit influence of diabatic heating within the SPCZ has, to the authors knowledge, not been investigated before. Following the SPCZ mechanism in the framework of Matthews (2012) and Van der Wiel *et al.* (2015a), an AGCM experiment has been designed in which the thermodynamical response to dynamical Rossby wave forcing is removed in the SPCZ region. Potential changes to the Rossby wave and the south Pacific mean flow will be investigated. In Section 2 the AGCM used in the experiments is described. The perturbation experiment is explained in more detail in Section 3. The results are described in Section 4 and finally the findings are summarised in Section 5.

2. Model description

The Intermediate General Circulation Model version 4 (IGCM4, Joshi *et al.* 2015) has been used in this study. It is an AGCM of intermediate complexity, i.e. within the hierarchy of climate models it has simpler parametrisation schemes than state-of-the-art AGCMs (e.g. the AGCMs in the Coupled Model Intercomparison Project phase 5, CMIP5). This makes the model well-suited for idealised experiments to increase process-level understanding.

IGCM4 is used here in its T42L20 configuration, i.e. 128 cells in longitude and 64 cells in latitude in the horizontal grid and 20 layers in the vertical. A monthly mean climatological seasonal cycle of SST, based on NOAA's Optimum Interpolation V2 dataset, is prescribed (Reynolds *et al.* 2002, mean over 1982-2009). Land surface temperatures are computed self-consistently from surface fluxes (Forster *et al.* 2000). IGCM4 runs the

Morcrette radiation scheme (Zhong & Haigh 1995) once for each model day. The parametrization for convective adjustment is based on the scheme of Betts (1986), it is slightly modified as described in Joshi *et al.* (2015). Cloud cover is computed to match observed profiles of convective clouds (Slingo 1987); there is no aerosol forcing. A more detailed description of the physical parametrizations in IGCM4 is given in Joshi *et al.* (2015).

The November to April time mean precipitation for observations and in the IGCM4 control integration are in good agreement (Figure 1). Data from the CPC merged analysis precipitation (CMAP) project have been used here as observations (Xie & Arkin 1997, mean over 1982-2009). Globally the quality of simulated precipitation in IGCM4 is within the range of CMIP5 atmosphere-only ('AMIP') experiments (Joshi *et al.* 2015). For the current study it is more relevant that SPCZ location and orientation are simulated well in IGCM4, though the simulated precipitation rate within the SPCZ is slightly lower than observed (Figure 1).

3. Experimental design

3.1. Control integration

The aim of the current paper is to investigate the influence of diabatic heating from convective activity in the SPCZ on other aspects of the Pacific climate. With this in mind we have designed a perturbation experiment in which SPCZ convective events are removed. The experiment is based on the transient wave - convection framework (Matthews 2012; Van der Wiel *et al.* 2015a). Figure 2 shows a flow diagram that depicts the consecutive steps in the experiment, each described in more detail below.

First, an IGCM4 control integration was conducted. This integration was 17 years long, from which the first year was removed as spin-up. The remaining 16 years of data contained 15 full November to April seasons (step 1 in Figure 2). Within these seasons, 140 SPCZ 'convective events' were selected, based on Empirical Orthogonal Functions (EOFs). EOF spatial patterns of variability were computed from daily anomalies of Outgoing Longwave Radiation (OLR) in a box over the SPCZ region (180°-120°W, 5°-30°S, rectangle in Figure 3). In the tropics, OLR can

1 156 be used as a proxy for precipitation; lower values are associated
2
3 157 with colder temperatures, higher cloud tops and enhanced deep
4
5 158 convection, higher values with warmer temperatures, lower cloud
6
7 159 tops and reduced deep convection. The Principle Component (PC)
8
9 160 time series associated with EOF 1 is then used for the selection of
10
11 161 the convective events. If the value of the PC was above 1 standard
12
13 162 deviation and was a local maximum relative to 5 days before and
14
15 163 5 days after that day, it was selected as a convective event (step 2
16
17 164 in Figure 2).

165 In the control integration, the computed temperature tendencies
166 in the deep convection routine were saved at every timestep.
167 These temperature tendency data were used to compute a three-
168 dimensional monthly varying climatology (step 3 in Figure 2), to
169 be used in the perturbation experiment.

3.2. Perturbation experiment

171 The perturbation experiment aims to prevent dynamical forcing
172 from Rossby waves from generating the observed anomalous
173 diabatic heating response in the SPCZ region (Matthews 2012;
174 Van der Wiel *et al.* 2015a). The experiment is based on 140
175 restart integrations started 4 days before each of the 140 selected
176 convective events in step 2. At this time (event -4 days) the
177 dynamical transient Rossby wave forcing is present, but the
178 convective response in the SPCZ region has not commenced.
179 From this atmospheric state a modified IGCM4 was integrated
180 for 14 days (i.e. up to 10 days after the event). In the
181 modified model all grid cells overlying ocean in the SPCZ
182 region (140°E-120°W, 0°-40°S, rectangle in Figure 1b) have
183 the deep convective temperature tendency prescribed from the
184 precalculated climatological tendency in step 3 rather than
185 computed self-consistently within the model code; i.e. instead
186 of allowing the deep convection scheme to compute temperature
187 tendencies, the climatological values were used. Moisture
188 tendencies and precipitation were computed as normal to avoid
189 an unrealistic build up or removal of moisture. Outside the SPCZ
190 region the model code was integrated as normal. The perturbation
191 experiment is the composite mean of all restart integrations (step 4
192 in Figure 2).

In the next section results from the different steps are discussed
separately. Steps 1 and 2 will be discussed in Subsection 4.1,
step 3 in 4.2 and finally step 4 in 4.3 and 4.4.

4. Experimental results

4.1. Transient wave - convection feedback in control integration

The first mode of variability from EOF analysis (7.8% of total
variance) shows enhanced convection (negative OLR anomalies)
shifted to the southwest, however it remains parallel to the
SPCZ mean precipitation axis (Figure 3a). To the northeast
a parallel band of reduced convection is found. The second
mode of variability (7.3%, not shown, well-separated from
EOF1 and further EOFs, North *et al.* 1982) shows enhanced
convection over the mean precipitation axis and reduced
convection to the southwest. These 'southwestward shifted' and
'enhanced' convection patterns are comparable to patterns found
in observational data (e.g. Vincent *et al.* 2011; Matthews 2012;
Salinger *et al.* 2014; Van der Wiel *et al.* 2015a).

Following the criteria presented in Section 3, 140 events of the
southwestward shifted mode have been selected from the EOF
1 PC time series (Figure 3b). Composite means were computed
by taking the mean of a field over all event days. Anomalies of
200 hPa vorticity and precipitation for these convective events are
shown in Figure 4. Four days before the event a Rossby wave
train is present south of Australia. As was found in observational-
based data, over the following days, the wave is refracted along
a curved path towards the equatorial east Pacific. During this
process the combined effect of advection by the mean wind,
shear on the equatorward edge of the jetstream and Rossby wave
refraction changes the shape of the vorticity centres (Van der
Wiel *et al.* 2015a); the centres develop a northwest-southeast
diagonal orientation, parallel to the SPCZ mean precipitation axis
(Figure 4b). This process is further supported by the meridional
stretching deformation of the basic state (Widlansky 2010).

Two days before the convective event the Rossby wave
initiates enhanced precipitation. Ahead of a cyclonic vorticity
anomaly, poleward wind ascends and in the tropical conditionally
unstable atmosphere this triggers deep convection. The vorticity
centre propagates northeastward with the Rossby wave, the

1 231 associated precipitation signal remains ahead of the cyclone at 270
 2 232 all times. At the day of the convective event, by design of the 271
 3 233 composite method, the precipitation anomaly reaches a maximum
 4 234 ($\sim 10 \text{ mm d}^{-1}$) and the pattern resembles the southwestward
 5 235 shifted pattern of EOF 1; there is a diagonal band of enhanced
 6 236 precipitation to the southwest of the SPCZ mean precipitation
 7 237 axis and reduced precipitation to the northeast. Two days after
 8 238 the convective event the precipitation anomalies have mostly
 9 239 disappeared (Figure 4d).

10 240 The diabatic heat release from the precipitation anomalies
 11 241 is substantial and enhances ascending motions and upper-
 12 242 tropospheric divergence. Through vortex stretching this acts as a
 13 243 negative feedback, $\partial\zeta/\partial t = -fD$, where ζ is relative vorticity,
 14 244 t is time, f is the Coriolis parameter and D is divergence,
 15 245 and results in an anticyclonic tendency: the propagating cyclone
 16 246 in the Rossby wave is dissipated. Consequently, Rossby wave
 17 247 propagation is disturbed downstream of the SPCZ region. The
 18 248 effect is clear in the evolution of the vorticity centres in the
 19 249 Rossby wave in Figure 4, at the moment precipitation anomalies
 20 250 are triggered propagation of the upstream cyclonic vorticity centre
 21 251 slows down and weakens. The Rossby wave favours a more
 22 252 southern propagation path, back towards the wave guide in the
 23 253 jet, where both precipitation anomalies and the negative feedback
 24 254 effect are weaker. Two days after the convective event the wave is
 25 255 mostly dissipated.

26 256 The sequence of events forcing diagonally oriented bands of
 27 257 precipitation in the IGCM4 control integration is similar to the
 28 258 sequence found using similar methods and observational-based
 29 259 data products (Matthews 2012; Van der Wiel *et al.* 2015a). The
 30 260 realistic representation of this process makes IGCM4 a suitable
 31 261 AGCM for the perturbation experiment.

32 262 4.2. Diabatic heating from deep convection

33 263 The simulated November to April time mean mid-tropospheric
 34 264 climatological heating due to deep convection is shown in
 35 265 Figure 5a. Higher values of diabatic heating are found at
 36 266 locations with frequent convective precipitation, lower values in
 37 267 areas of less precipitation (Figures 1b, 5a). The SPCZ, ITCZ,
 38 268 South Atlantic Convergence Zone (SACZ) and South Indian
 39 269 Convergence Zone can all be identified as areas of enhanced

diabatic heating from deep convection. The south Pacific dry zone
 has very weak diabatic heating from deep convection.

Figures 5b,c show vertical sections of the same quantity. The
 black areas on the cross-section show the grid cells where the
 IGCM4 deep convection scheme has not once been initiated in
 the 15 seasons included in the control integration (effectively
 the stratosphere). For these cells a climatological heating of
 $0 \text{ K timestep}^{-1}$ is assumed in the experimental integration. Along
 155°E (Figure 5b) the region of most intense heating lies over the
 equator, where the SPCZ and ITCZ merge. In this region, there
 is a slight negative temperature tendency at the surface due to
 evaporative cooling, in the mid-troposphere there is substantial
 diabatic heating and near the model top ($\sigma=0.05$) there is a
 negative temperature tendency due to radiative cooling. Further
 east at 149°W (Figure 5c) the heating profiles related to the SPCZ
 and ITCZ are weaker and separated and found at about 20°S and
 8°N respectively.

These climatological temperature tendency data are used
 in the perturbation experiment. Instantaneous, self-consistent
 temperature tendencies are used in the control integration (left
 column of Figure 6). This heating pattern is more irregular than
 in the climatology, changes fast in time and has larger extremes.
 Following the earlier discussion, it can be seen that ahead
 of upper-tropospheric cyclonic vorticity anomalies convective
 heating is strongest. As the cyclone propagates northeastward this
 region of enhanced heating also moves northeastward, similar
 to the progression of precipitation anomalies (Figure 4). Ahead
 of anticyclonic vorticity anomalies convective heating is weaker.
 In the perturbation experiment, as discussed in Section 3, in
 the SPCZ region this instantaneous, self-consistent temperature
 tendency is replaced by the relevant climatological value from the
 seasonal cycle appropriate for each of the 140 restart integrations.
 The composite mean temperature tendencies as used in the
 experimental model integration are shown in the right column of
 Figure 6. Outside the rectangular SPCZ region there has been
 no change from the control integration (small differences due
 to separate integrations in control and experiment), inside the
 rectangular region instantaneous values have been replaced by
 climatological values (compare horizontal rows in Figure 6).

4.3. Impact of diabatic heating on Rossby wave propagation

As described in Section 3, the restart integrations are initiated from the control integration at 4 days before the 140 selected convective events. At this moment a Rossby wave train is present south of Australia (Figure 7a). Two days into the perturbation experiment, the Rossby wave has propagated northeastward into the SPCZ region (Figure 7b). Ahead of the cyclonic anomaly is an anomalous poleward flow that leads to ascent along the sloping mean isentropes. There is a small anomalous precipitation signal associated with this ascent ($\sim 2 \text{ mm d}^{-1}$). However, the associated anomalous diabatic heat release is removed in the experiment so no additional ascending motions are forced. This results in a much weaker precipitation rate in the perturbation experiment than in the control integration at this point ($\sim 8 \text{ mm d}^{-1}$, Figure 4b).

In the following days this process continues. Vorticity centres in the wave propagate northeastward. Ahead of the cyclonic vorticity anomaly and along the SPCZ mean precipitation axis there is some anomalous precipitation. However, the precipitation rates are constant around $\sim 2 \text{ mm d}^{-1}$; there is no distinct peak in precipitation rates at the convective event as was found in the control integration.

In the sequence of events that ultimately triggers diagonal bands of convective precipitation over the SPCZ region in the control integration, the negative feedback from vortex stretching starts influencing Rossby wave propagation two days before the convective event. When the convective heating response is taken out of the sequence, diabatic heating, ascending motions and upper-tropospheric divergence are all significantly weaker than in the control integration. The maximum composite-mean upper-tropospheric divergence in the perturbation experiment is $4 \times 10^{-6} \text{ s}^{-1}$, only 30% of the divergence in the control integration ($13 \times 10^{-6} \text{ s}^{-1}$). The negative feedback, $\partial\zeta/\partial t = -fD$, is therefore much weaker and has a smaller effect on the transient Rossby wave.

The northeastward propagation of the Rossby wave is undisturbed in the perturbation experiment. The vorticity centres are reformed due to shear and Rossby refraction as in the control integration, though the effects are more obvious in the experiment.

Vorticity centres become elongated and rotate from a diagonal orientation (northwest-southeast) to a zonal orientation at the equator (Figure 7c). The southward tendency of the wave pattern in the control integration is not found in the experiment, instead Rossby wave propagation continues across the equator.

The propagation speed of the Rossby wave can be estimated from a Hovmöller diagram (Figure 8). The vorticity centres move eastward steadily at the phase speed; wave energy moves through the region at the faster group speed. In the perturbation experiment the phase speed is about $580 \text{ km d}^{-1} \approx 6.7 \text{ m s}^{-1}$, the group speed approximately $2000 \text{ km d}^{-1} \approx 23 \text{ m s}^{-1}$ (grey dotted lines in Figure 8). These values are comparable in the control integration, however wave propagation downstream of the SPCZ mean precipitation axis is disturbed. The cyclone at 180° weakens when precipitation is triggered 2 days before the convective event, in the perturbation experiment the cyclone is present for longer and propagates further eastward. The same effect appears for the anticyclone at 160°W . In both model integrations propagation slows down close to the equator at about 130°W . Not visible in the Hovmöller diagram is the different shape of the Rossby waves after the convective events in the control integration and perturbation experiment (Figures 4d and 7d).

As precipitation rates decrease significantly in the perturbation experiment, there is a slight build up of moisture in the experimental region of up to 2 g kg^{-1} in specific humidity at 850 hPa. This moisture is advected by horizontal winds out of the experimental region. This results in enhanced precipitation over New Guinea and in a zonal line just north of the experimental region (Figures 7c,d), as the model computes convective temperature tendencies self-consistently there. The increased moisture content does increase modelled low level clouds and through a radiative feedback lowers surface temperatures in the SPCZ region slightly. The impact of this side effect on Rossby wave propagation in the experimental region is small.

4.4. Impact of diabatic heating on the mean flow

Six days after the convective event the Rossby wave has disappeared in both the control integration and in the perturbation experiment. In the control integration the upper troposphere has returned to its 'normal' state (Figure 9a); anomalies of zonal wind

speed are very small (less than 2 m s^{-1}). There is no coherent pattern to these anomalies over most of the Pacific Ocean, though there is a hint of a wave train over South America, from the southeast Pacific towards the equatorial Atlantic. A similar wave train has been linked to enhanced SACZ activity (e.g. Liebmann *et al.* 1999; Robertson & Mechoso 2000; Van der Wiel *et al.* 2015a). By means of influence functions, Grimm & Silva Dias (1995) found a link between convection in the SPCZ and in the SACZ. However, no significant lagged correlations were found between convective events in the SPCZ and subsequent convective events in the SACZ in the IGCM4 control integration.

The post-convective event upper tropospheric zonal wind anomalies in the perturbation experiment are much larger (Figure 9b). Along the Rossby wave propagation path and over the equatorial east Pacific there are strong positive (westerly) anomalies. To the north and south of the propagation path there are negative (easterly) anomalies. The anomaly pattern is approximately southwest-northeast, perpendicular to the prescribed heating pattern, which suggests it is not a direct effect in response to the prescribed heating but rather has a different, dynamical origin.

In the control integration and in the actual climate system, there are two processes that feedback from SPCZ activity onto the basic state wind. In general, tropical heating results in an off-equatorial anticyclone that accelerates the subtropical jets, through a Gill-like response (Gill 1980). Additionally, the diagonal, northwest-southeast, orientation of the vorticity centres in the waves leads to a mean poleward transport of westerly momentum in these waves, as anomalies of the zonal and meridional wind are anticorrelated in the wave ($\overline{u'v'} < 0$, see also Kiladis 1998). These two processes determine, in part, the strength of the modelled climatological subtropical jet at 30°S . The Gill-response and momentum transport by Rossby waves in the control run result in this climatological jet. The weak anomalies after the SPCZ events (Figure 9a) are just due to sampling variability.

In the perturbation experiment both processes are modified. Diabatic heating in the SPCZ region is limited, therefore the Gill anticyclone would be weaker and its acceleration of the subtropical jet would be decreased. However, this is not observed in the experiment (Figure 9b); the effect is off-set by the

strengthened Rossby wave signal. Rossby wave propagation towards the SPCZ region and the westerly duct is enhanced, leading to increased poleward transport of westerly momentum and positive anomalies of zonal wind in the subtropical jet. Rossby wave propagation from the SPCZ region back towards the subtropical jet is less favoured in this state, resulting in weaker poleward momentum transport and negative zonal wind anomalies at 40°S , 120°W .

In the perturbation experiment the anomalous diabatic heating from SPCZ convection triggered by equatorward propagating Rossby waves has been switched *off*. Therefore, the climatological effect of this SPCZ convection on the basic state (contours in Figure 9c) will be the *opposite* of the effect in the perturbation experiment (Figure 9b). Dashed contours in Figure 9c show areas where the climatological westerly winds are decreased in strength or where climatological easterly winds are increased in strength; solid contours show areas of increased westerly/decreased easterly winds. Therefore, convective events in the SPCZ act to decrease the strength of the subtropical jet and the westerly winds along the wave propagation path. This results in an enhancement of the region of negative stretching deformation near the SPCZ. Following the mechanism discussed in Widlansky *et al.* (2011), this would increase the accumulation of wave energy there and increase convection along the SPCZ. The described feedback would be positive: convective events in the SPCZ increase the likelihood of further convective events.

Furthermore, the strength of the westerly duct over the equatorial eastern Pacific is decreased. The westerly duct is partially responsible for the initial equatorward propagation of the Rossby waves. In the IGCM4 control integration the zonal wind speed in the westerly duct is $\sim 20 \text{ m s}^{-1}$ (colours in Figure 9c), a change of $\sim -4 \text{ m s}^{-1}$ due to SPCZ convection is an important factor in determining its strength. This feedback would be negative: convective events in the SPCZ decrease the likelihood of wave refraction towards the SPCZ and the westerly duct, decreasing the chance of a next convective event.

5. Discussion

The influence of convective events in the SPCZ on local Rossby wave propagation and the Pacific mean flow has been

1 466 tested by means of an AGCM experiment. In observational
 2 467 data and in the control integration, Rossby waves trigger deep
 3 468 convection and precipitation in the SPCZ. In a perturbation
 4 469 experiment the dynamical Rossby wave forcing is decoupled from
 5 470 a potential thermodynamical response: instantaneous diabatic
 6 471 heating during SPCZ convective events is removed and replaced
 7 472 by a climatological value. Experimental results show continued
 8 473 Rossby wave propagation from the subtropical jet towards
 9 474 the eastern equatorial Pacific and across the equator. In the
 10 475 control integration and in observations these Rossby waves are
 11 476 dissipated in the SPCZ region due to diabatic heat release in
 12 477 the convection and a negative feedback due to vortex stretching.
 13 478 The continued Rossby propagation in the experiment provides
 14 479 additional evidence for the feedback mechanism in the transient
 15 480 wave-convection framework proposed by Matthews (2012) and
 16 481 Van der Wiel *et al.* (2015a).

17 482 Besides influencing transient Rossby waves locally, the
 18 483 experiment shows convective events in the SPCZ region have a
 19 484 significant impact on the south Pacific upper-tropospheric zonal
 20 485 wind climate. As discussed, in the control integration and in
 21 486 observations, convective events in the SPCZ hinder Rossby wave
 22 487 propagation in the region. Consequently the poleward transport of
 23 488 westerly momentum is decreased, as transient Rossby waves are
 24 489 an important factor in the tropical momentum balance (Kiladis
 25 490 1998). Convective events in the SPCZ act to weaken both the
 26 491 subtropical jet and the equatorial westerly duct. The first of
 27 492 these effects enhances the region of negative zonal stretching
 28 493 deformation potentially resulting in enhanced convection along
 29 494 the SPCZ (Widlansky *et al.* 2011). The second reduces the
 30 495 equatorward refraction of Rossby waves that trigger SPCZ
 31 496 convective events (Van der Wiel *et al.* 2015a). To determine
 32 497 the strength of these feedbacks requires further modelling
 33 498 experiments.

34 499 These results can be interpreted within the general framework
 35 500 of Meehl *et al.* (2001), where atmospheric processes on longer
 36 501 time scales and larger spatial scales set a mean atmospheric state
 37 502 on which synoptic waves propagate (the Rossby waves in the
 38 503 SPCZ in this example). In the general framework, processes on
 39 504 synoptic scales then influence atmospheric processes on synoptic
 40 505 time scales, but also on longer time and larger spatial scales.

506 Here, this corresponds to the effect convective activity has on the
 507 atmospheric basic state through changed momentum transport.
 508 SST biases in coupled models in the Coupled Model
 509 Intercomparison Project phase 5 (CMIP5) force a too zonal
 510 tropical part of the SPCZ, which then gives a more discontinuous
 511 simulated SPCZ than is observed (Brown *et al.* 2011, 2013; Niznik
 512 *et al.* 2015). Such biases influence future rainfall projections of
 513 the SPCZ (Widlansky *et al.* 2013). Based on the results presented
 514 here, biases in the represented SPCZ lead to further biases in the
 515 representation of convective heating, Rossby wave propagation,
 516 momentum transport and the mean upper-tropospheric wind
 517 climate. Projections of changes in atmospheric processes in a
 518 future warmer climate are often based on these CMIP5 models,
 519 it is therefore of importance to improve the representation of the
 520 SPCZ in such models.

Acknowledgements

521 The CMAP data were provided by the NOAA/OAR/ESRL
 522 PSD, Boulder, Colorado, USA, from their web site at
 523 <http://www.cdc.noaa.gov/>. The research presented in this article
 524 was carried out on the High Performance Computing Cluster
 525 supported by the Research Computing Service at the University of
 526 East Anglia. The authors would like to thank George Kiladis and
 527 three anonymous reviewers for comments that helped to improve
 528 the manuscript.

References

- 529
 530
 531 Ambrizzi, T, Hoskins, B J, & Hsu, H-H. 1995. Rossby wave propagation and
 532 teleconnection patterns in the austral winter. *Journal of the Atmospheric
 533 Sciences*, **52**, 3661 – 3672.
 534 Betts, A K. 1986. A new convective adjustment scheme. Part I: Observational
 535 and theoretical basis. *Quarterly Journal of the Royal Meteorological
 536 Society*, **112**, 677 – 691.
 537 Brown, J R, Power, S B, Delage, F P, Colman, R A, Moise, A F, & Murphy,
 538 B F. 2011. Evaluation of the South Pacific Convergence Zone in IPCC AR4
 539 climate model simulations of the twentieth century. *Journal of Climate*, **24**,
 540 1565 – 1582.
 541 Brown, J R, Moise, A F, & Colman, R A. 2013. The South Pacific Convergence
 542 Zone in CMIP5 simulations of historical and future climate. *Climate
 543 Dynamics*, **41**, 2179 – 2197.
 544 Cai, W, Lengaigne, M, Borlace, S, Collins, M, Cowan, T, McPhaden, M J,
 545 Timmermann, A, Power, S, Brown, J, Menkes, C, Ngari, A, Vincent, E M,

- 1 546 & Widlansky, M J. 2012. More extreme swings of the South Pacific
2 Convergence Zone due to greenhouse warming. *Nature*, **488**, 365 – 370. 593
- 3 547
4 Forster, P M de F, Blackburn, M, Glover, R, & Shine, K P. 2000. An
5 examination of climate sensitivity for idealised climate change experiments
6 in an intermediate general circulation model. *Climate Dynamics*, **16**, 833 –
7 550
8 849. 594
- 9
10 Gill, A E. 1980. Some simple solutions for heat-induced tropical circulation.
11 *Quarterly Journal of the Royal Meteorological Society*, **106**, 447 – 462. 595
- 12 554
13 Griffiths, G M, Salinger, M H, & Leleu, I. 2003. Trends in extreme daily
14 rainfall across the South Pacific and relationship to the South Pacific
15 Convergence Zone. *International Journal of Climatology*, **23**, 847 – 869. 596
- 16 556
17 Grimm, A M, & Silva Dias, P L. 1995. Analysis of tropical-extratropical
18 interactions with influence functions of a barotropic model. *Journal of the
19 Atmospheric Sciences*, **52**, 3538 – 3555. 597
- 20 559
21 Haffke, C, & Magnusdottir, G. 2013. The South Pacific Convergence Zone in
22 three decades of satellite images. *Journal of Geophysical Research*, **118**, 1
23 – 11. 598
- 24 562
25 Hoskins, B J, & Ambrizzi, T. 1993. Rossby wave propagation on a realistic
26 longitudinally varying flow. *Journal of Atmospheric Sciences*, **50**, 797 –
27 812. 599
- 28 565
29 Hoskins, B J, James, I N, & White, G H. 1983. The shape, propagation
30 and mean-flow interaction of large-scale weather systems. *Journal of the
31 Atmospheric Sciences*, **40**, 1595 – 1612. 600
- 32 568
33 Hubert, L F. 1961. A subtropical convergence line of the South Pacific: a case
34 study using meteorological satellite data. *Journal of Geophysical Research*,
35 **66**, 1661 – 1671. 601
- 36 571
37 Jin, F, & Hoskins, B J. 1995. The direct response to tropical heating in a
38 baroclinic atmosphere. *Journal of the Atmospheric Sciences*, **52**, 307 – 319. 602
- 39 573
40 Joshi, M M, Stringer, M, Van der Wiel, K, O'Callaghan, A, & Fueglistaler,
41 S. 2015. IGC4: a fast, parallel and flexible intermediate climate model.
42 *Geoscientific Model Development*, **8**, 1157–1167. 603
- 43 576
44 Kiladis, G N. 1998. Observations of Rossby waves linked to convection over
45 the eastern tropical Pacific. *Journal of Atmospheric Sciences*, **55**, 321 –
46 339. 604
- 47 579
48 Kiladis, G N, & Weickmann, K M. 1992. Extratropical forcing of tropical
49 Pacific convection during northern winter. *Monthly Weather Review*, **120**,
50 1924 – 1938. 605
- 51 582
52 Kiladis, G N, & Weickmann, K M. 1997. Horizontal structure and seasonality
53 of large-scale circulations associated with submonthly tropical convection.
54 *Monthly Weather Review*, **125**, 1997–2013. 606
- 55 585
56 Kiladis, G N, von Storch, H, & van Loon, H. 1989. Origin of the South Pacific
57 Convergence Zone. *Journal of Climate*, **2**, 1185 – 1195. 607
- 58 587
59 Kumar, V V, Deo, R C, & Ramachandran, V. 2006. Total rain accumulation
60 and rain-rate analysis for small tropical Pacific islands: a case study of Suva,
589 Fiji. *Atmospheric Science Letters*, **7**, 53 – 58. 608
- 590
591 Liebmann, B, Kiladis, G N, Marengo, J A, Ambrizzi, T, & Glick, J D.
592 1999. Submonthly convective variability over South America and the South
Atlantic convergence zone. *Journal of Climate*, **12**, 1877 – 1891. 593
- Lintner, B R, & Neelin, J D. 2008. Eastern margin variability of the South
Pacific Convergence Zone. *Geophysical Research Letters*, **35**, L16701. 594
- Matsuno, T. 1966. Quasi-Geostrophic motions in the equatorial area. *Journal
of the Meteorological Society of Japan*, **44**, 25 – 42. 595
- 596
597
598
599
600
601
602
603
604
605
606
607
608
609
610
611
612
613
614
615
616
617
618
619
620
621
622
623
624
625
626
627
628
629
630
631
632
633
634
635
636
637
638

- 1 639 Streten, N A. 1973. Some characteristics of satellite-observed bands of
2 640 persistent cloudiness over the Southern Hemisphere. *Monthly Weather*
3 641 *Review*, **101**, 486 – 495.
- 5 642 Takahashi, K, & Battisti, D S. 2007a. Processes controlling the mean tropical
6 643 Pacific precipitation pattern. Part I: The Andes and the Eastern Pacific
7 644 ITCZ. *Journal of Climate*, **20**, 3434 – 3451.
- 9 645 Takahashi, K, & Battisti, D S. 2007b. Processes controlling the mean tropical
10 646 Pacific precipitation pattern. Part II: the SPCZ and the southeast Pacific dry
11 647 zone. *Journal of Climate*, **20**, 5696 – 5706.
- 13 648 Trenberth, K E. 1976. Spatial and temporal variations of the Southern
14 649 Oscillation. *Quarterly Journal of the Royal Meteorological Society*, **102**,
15 650 639 – 653.
- 17 651 Van der Wiel, K, Matthews, A J, Stevens, D P, & Joshi, M M. 2015a. A
18 652 dynamical framework for the origin of the diagonal South Pacific and
19 653 South Atlantic Convergence Zones. *Quarterly Journal of the Royal*
20 654 *Meteorological Society*. published online, doi: 10.1002/qj.2508.
- 22 655 Van der Wiel, K, Matthews, A J, Joshi, M M, & Stevens, D P. 2015b. Why the
23 656 South Pacific Convergence Zone is diagonal. *Climate Dynamics*. published
24 657 online, doi: 10.1007/s00382-015-2668-0.
- 26 658 Vincent, D G. 1994. The South Pacific Convergence Zone (SPCZ): a review.
27 659 *Monthly Weather Review*, **122**, 1949 – 1970.
- 29 660 Vincent, E M, Lengaigne, M, Menkes, C E, Jourdain, N C, Marchesiello, P, &
30 661 Madec, G. 2011. Interannual variability of the South Pacific Convergence
31 662 Zone and implications for tropical cyclone genesis. *Climate Dynamics*, **36**,
32 663 1881 – 1896.
- 34 664 Widlansky, M J. 2010. *Climate dynamics of the South Pacific Convergence*
35 665 *Zone and similarities with other subtropical convergence zones in the*
36 666 *southern hemisphere*. Ph.D. thesis, Georgia Institute of Technology.
- 38 667 Widlansky, M J, Webster, P J, & Hoyos, C D. 2011. On the location and
39 668 orientation of the South Pacific Convergence Zone. *Climate Dynamics*, **36**,
40 669 561 – 578.
- 42 670 Widlansky, M J, Timmermann, A, Stein, K, McGregor, S, Schneider, N,
43 671 England, M H, Lengaigne, M, & Cai, W. 2013. Changes in South Pacific
44 672 rainfall bands in a warming climate. *Nature Climate Change*, **3**, 417 – 423.
- 46 673 Xie, P, & Arkin, P A. 1997. Global precipitation: a 17-year monthly analysis
47 674 based on gauge observations, satellite estimates, and numerical model
48 675 outputs. *Bulletin of the American Meteorological Society*, **78**, 2539 – 2558.
- 50 676 Zhong, W Y, & Haigh, J D. 1995. Improved broad-band emissivity
51 677 parameterization for water vapor cooling calculations. *Journal of*
52 678 *Atmospheric Sciences*, **52**, 124 – 138.

1
2
3
4
5
6
7
8
9
10
11
12
13
14
15
16
17
18
19
20
21
22
23
24
25
26
27
28
29
30
31
32
33
34
35
36
37
38
39
40
41
42
43
44
45
46
47
48
49
50
51
52
53
54
55
56
57
58
59
60

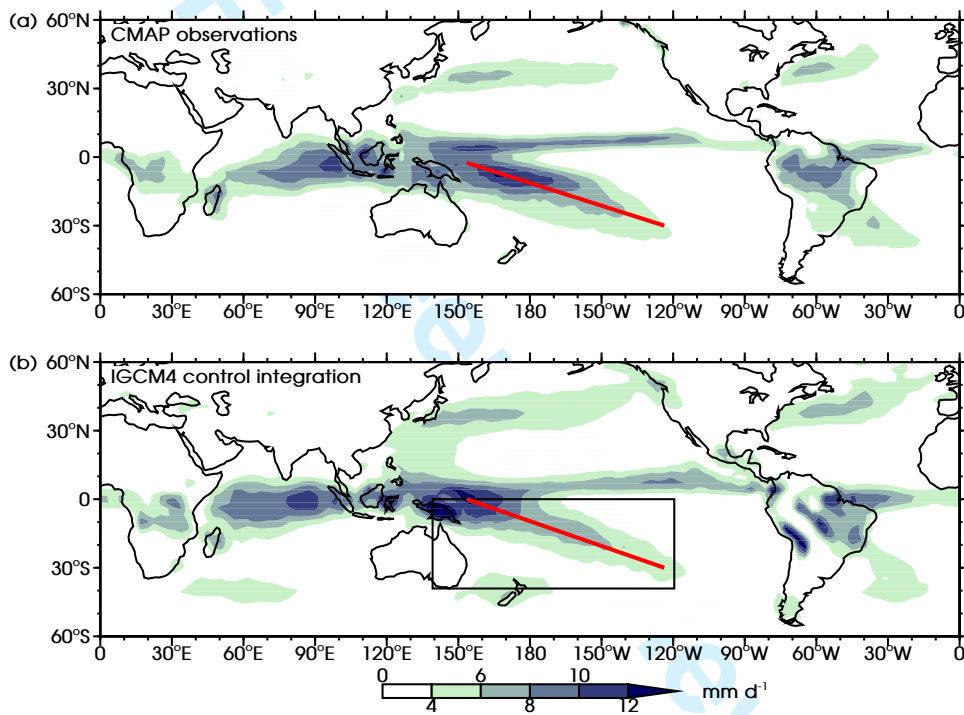


Figure 1. Time mean precipitation rate (November to April) in (a) CMAP and (b) the IGCM4 control integration (mm d^{-1}). The thick diagonal red lines show the position of the mean SPCZ precipitation axis, the rectangle in (b) shows the region for the perturbation experiment.

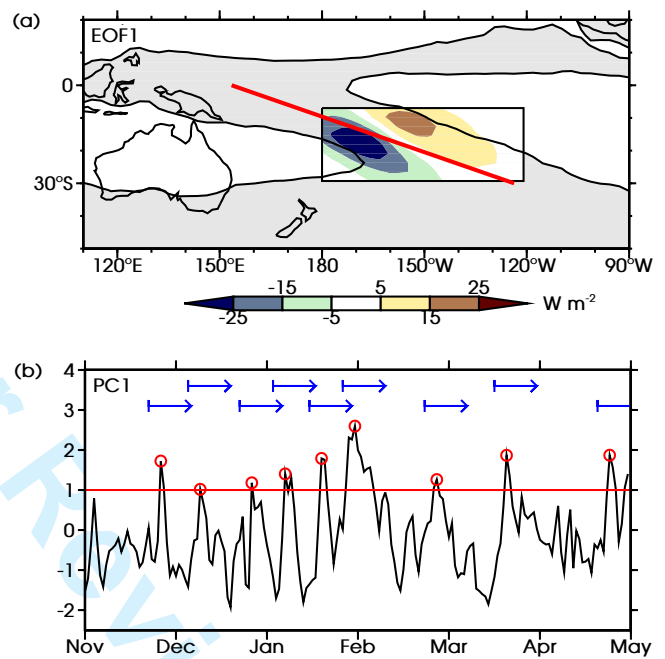
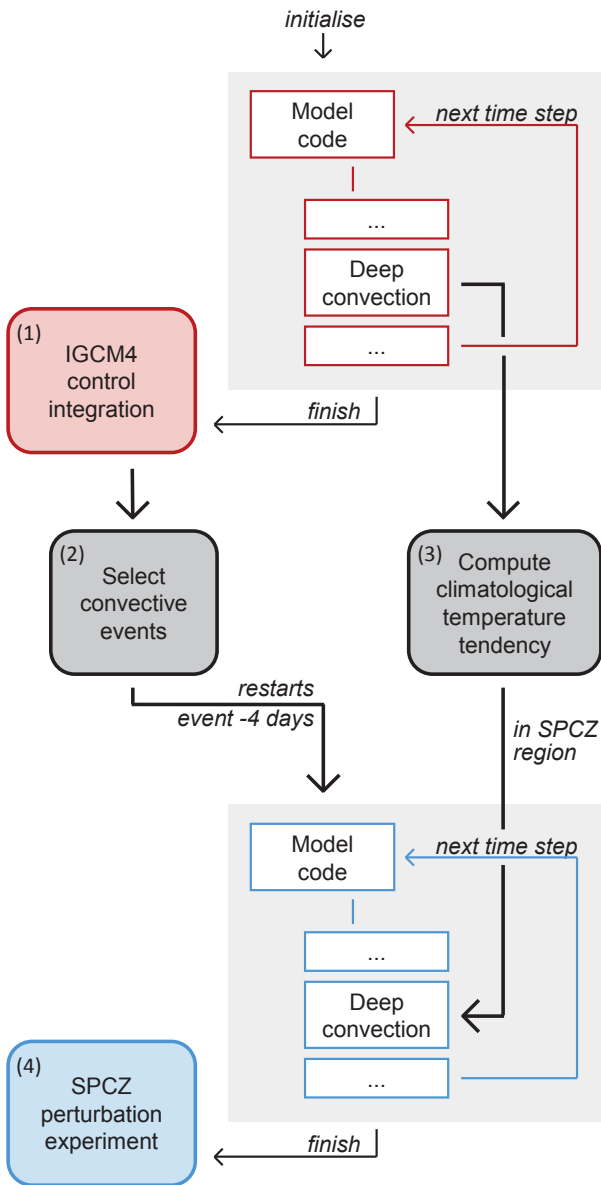


Figure 3. (a) EOF pattern 1 in shaded colours ($W m^{-2}$) in the rectangular box, overlaid on the time mean OLR field (November to April, grey shading is $< 250 W m^{-2}$). The thick diagonal red line shows the position of the SPCZ mean precipitation axis. (b) Sample time series of the PC associated with EOF 1 during November-April of model integration year 10. The red line and circles show the selection of SPCZ convective events, blue arrows show the duration of the associated restart integrations.

Figure 2. Flow diagram of experimental setup; detailed explanations of each step numbered (1) through (4) are provided in the main text (Section 3).

1
2
3
4
5
6
7
8
9
10
11
12
13
14
15
16
17
18
19
20
21
22
23
24
25
26
27
28
29
30
31
32
33
34
35
36
37
38
39
40
41
42
43
44
45
46
47
48
49
50
51
52
53
54
55
56
57
58
59
60

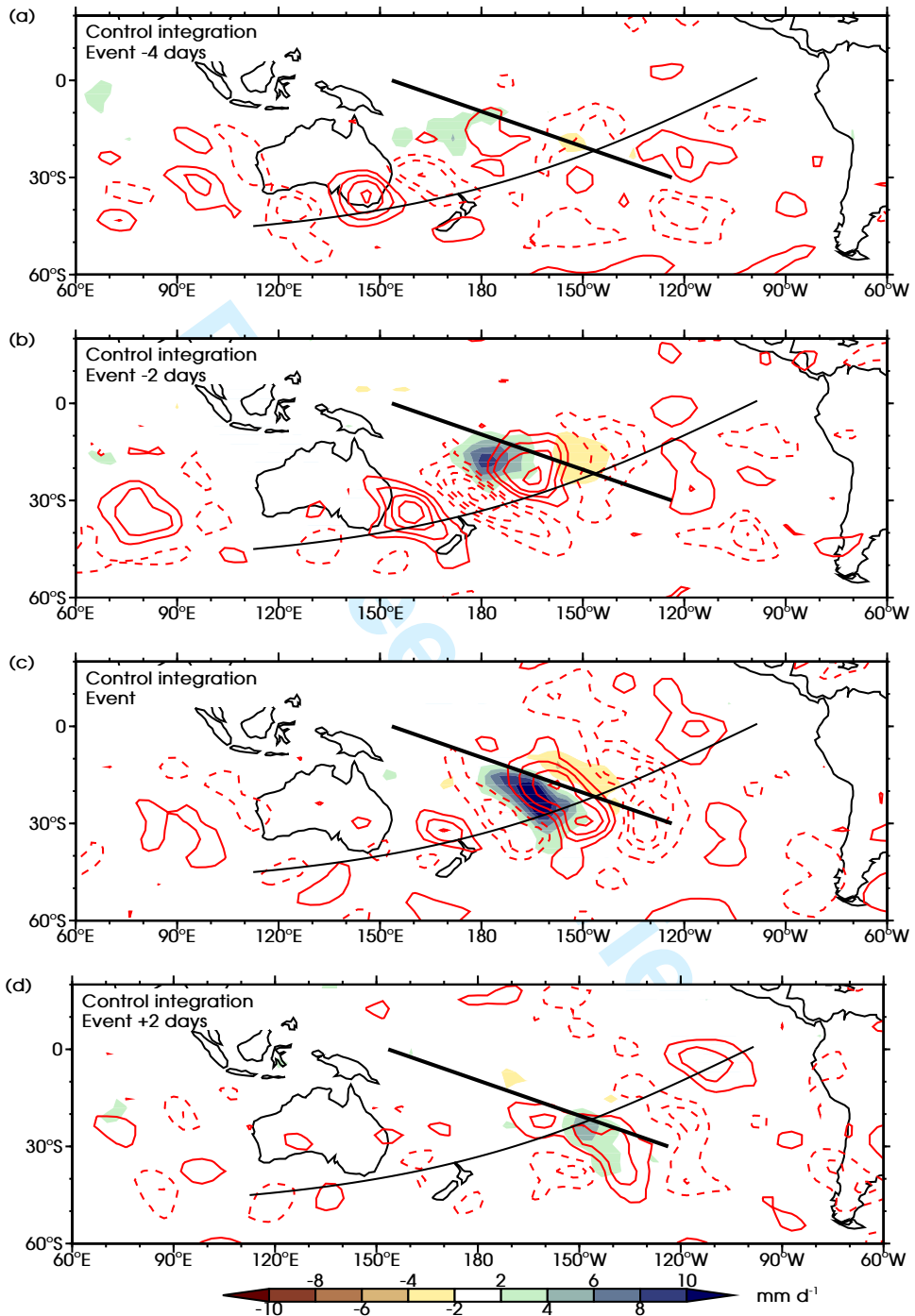


Figure 4. Composite mean anomalies over the 140 shifted SPCZ events of precipitation rate in shaded colours (mm d⁻¹), and 200 hPa vorticity in red contours ($4 \times 10^{-6} \text{ s}^{-1}$ contour interval, zero contour omitted, negative contours dashed) for the ICGM4 control integration. The thick diagonal line indicates the position of the SPCZ mean precipitation axis, the curved line an approximate wave propagation path. Time lags shown: (a) event -4 days, (b) event -2 days, (c) event, and (d) event +2 days.

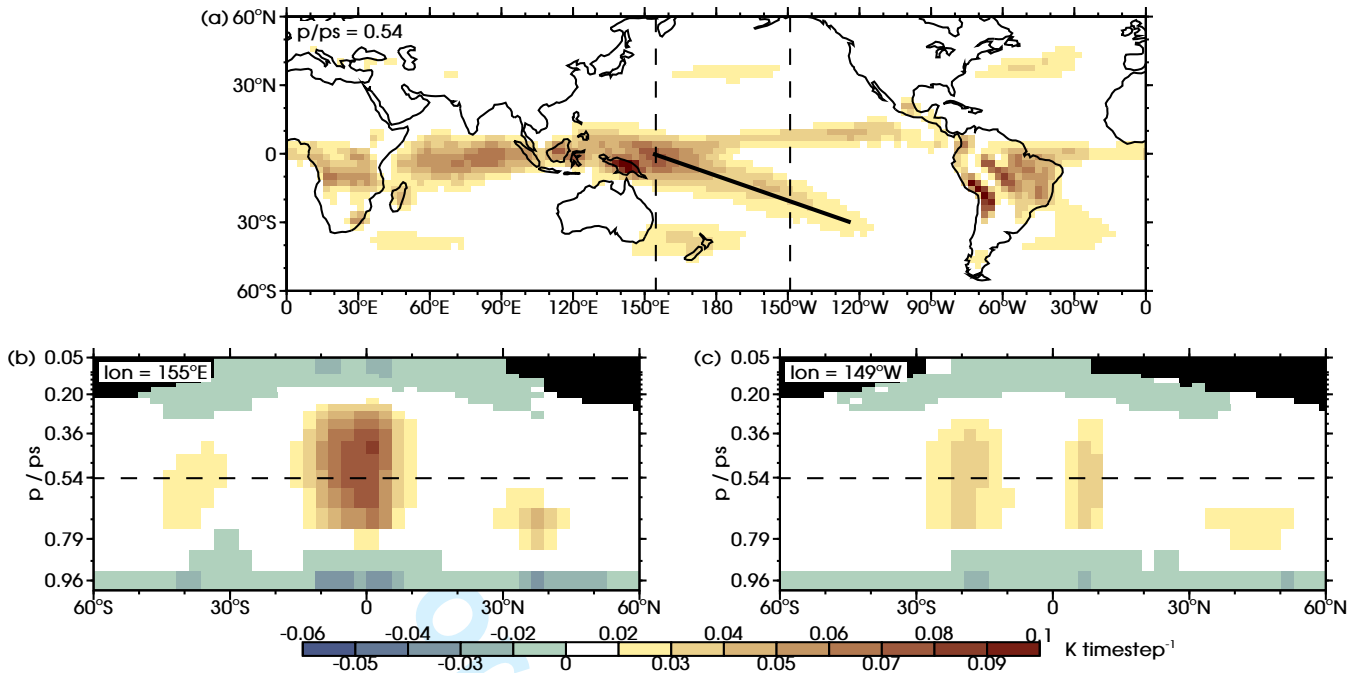


Figure 5. Time mean temperature tendency due to deep convection (November to April) in ICGM4 at (a) $p/ps = 0.54$, and vertical sections at (b) 155°E and (c) 149°W in shaded colours (K timestep^{-1}). Vertical levels are pressure (p) / surface pressure (ps) or sigma coordinates. Dashed lines in (a) show the locations of the vertical sections in (b,c), dashed lines in (b,c) show the level of the map in (a). The thick diagonal line in (a) shows the position of the mean SPCZ precipitation axis. Black areas signify areas where data is not available.

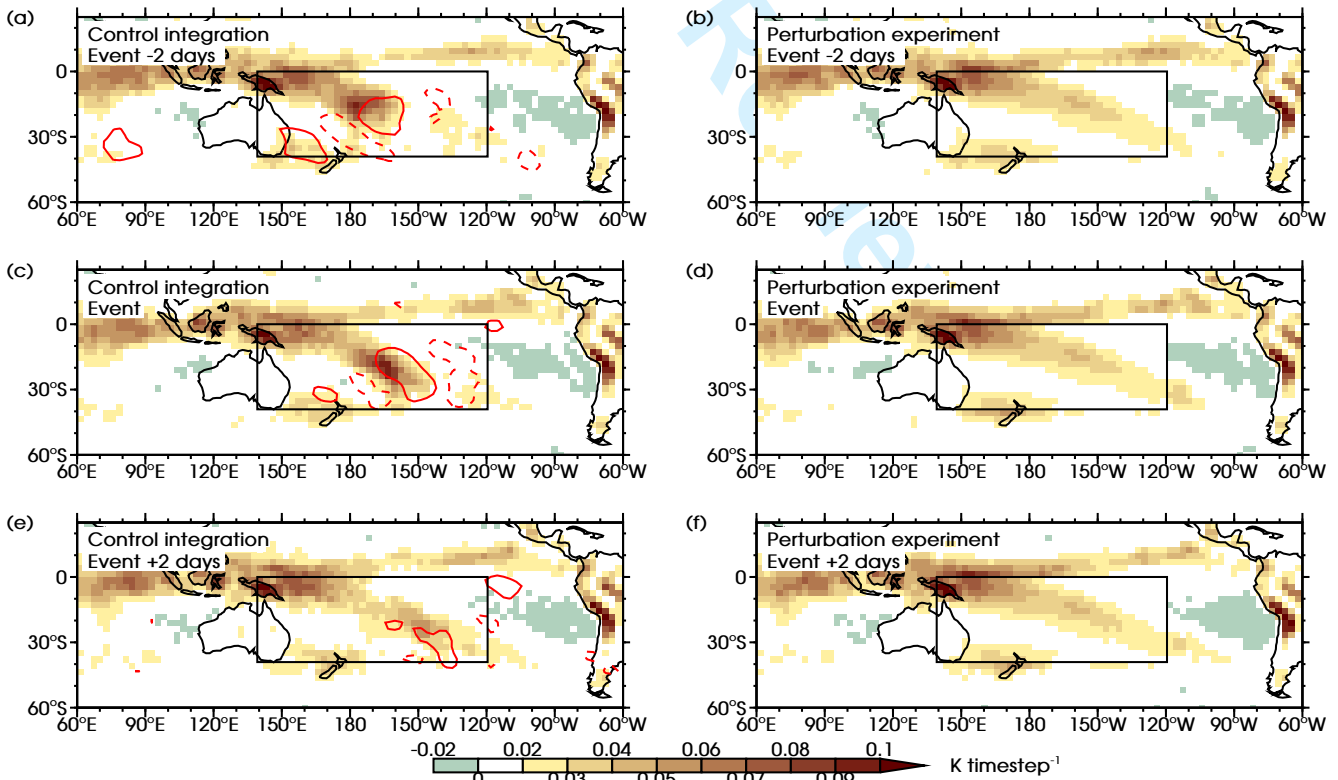


Figure 6. Composite mean temperature tendency due to deep convection at $\sigma = 0.54$ in shaded colours (K timestep^{-1}). (a,c,e) show the instantaneous, self-consistent model computed tendency in the control integration. In the perturbation experiment this is replaced by the climatological tendency within the experiment region (black rectangle) as shown in (b,d,f). Red contours in (a,c,e) show 200 hPa vorticity anomalies in the control integration (as in Figure 4, the $8 \times 10^{-6} \text{ s}^{-1}$ contour as a solid line, the $-8 \times 10^{-6} \text{ s}^{-1}$ contour as a dashed line).

1
2
3
4
5
6
7
8
9
10
11
12
13
14
15
16
17
18
19
20
21
22
23
24
25
26
27
28
29
30
31
32
33
34
35
36
37
38
39
40
41
42
43
44
45
46
47
48
49
50
51
52
53
54
55
56
57
58
59
60

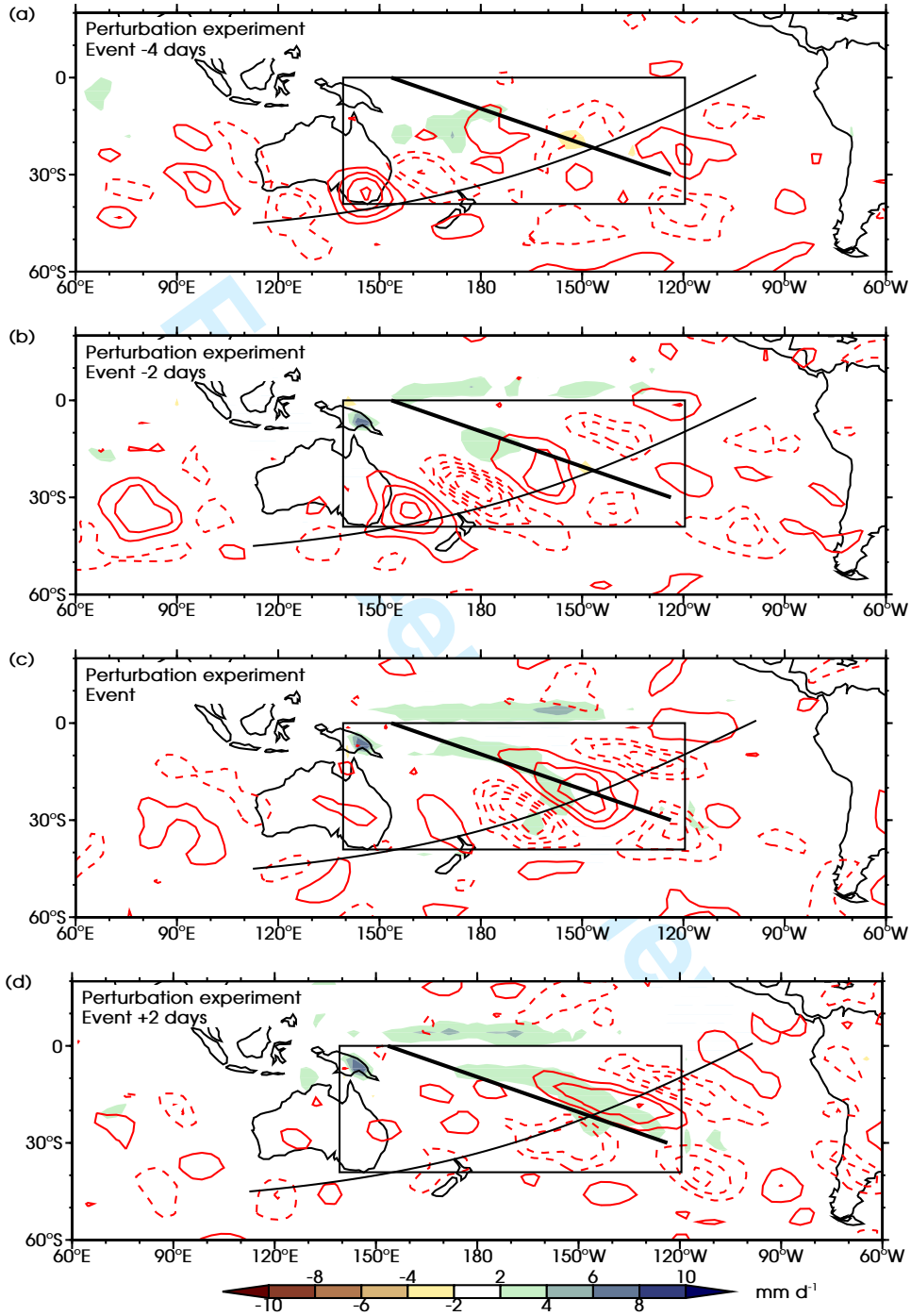


Figure 7. As Figure 4, but for the perturbation experiment. Note (a) is the same as Figure 4a, the starting point of the perturbation experiment. The rectangle indicates the region for the perturbation experiment.

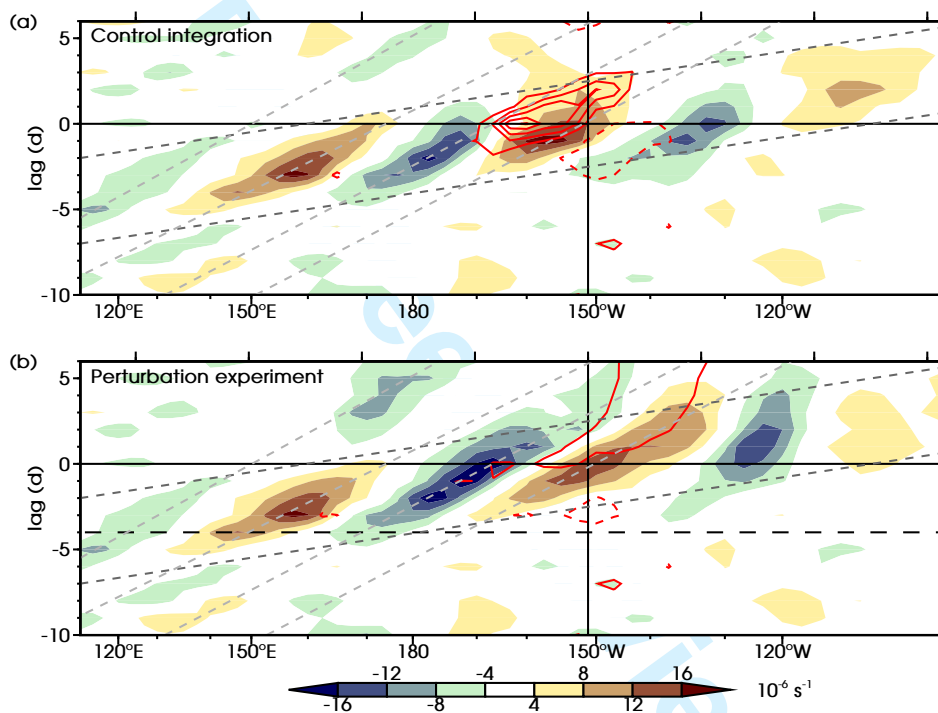


Figure 8. Hovmöller diagram of lagged composite anomalies along the curved propagation path in the (a) control integration (Figure 4) and (b) perturbation experiment (Figure 7). The 200 hPa vorticity is shown in shaded colours (10^{-6} s^{-1}) and precipitation in red contours (2 mm d^{-1} contour interval, zero contour omitted, negative contours dashed). The vertical solid line denotes the position of the mean SPCZ axis, the horizontal dashed line in (b) is the beginning of the restart integrations at event -4 days. Light grey dotted lines show the approximate phase speed, dark grey dotted lines the approximate group speed. Horizontal axes are irregular longitude (bottom) or regular distance (top, 2000 km intervals) along the path.

1
2
3
4
5
6
7
8
9
10
11
12
13
14
15
16
17
18
19
20
21
22
23
24
25
26
27
28
29
30
31
32
33
34
35
36
37
38
39
40
41
42
43
44
45
46
47
48
49
50
51
52
53
54
55
56
57
58
59
60

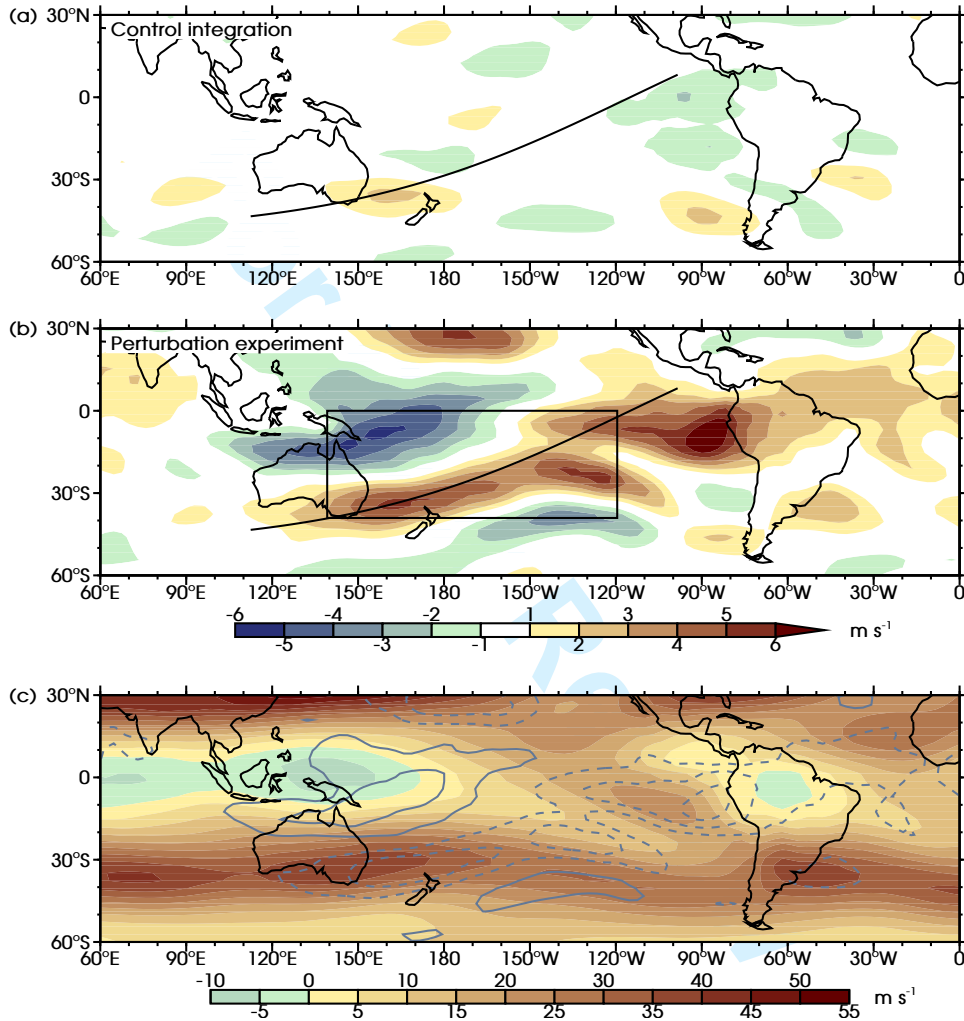


Figure 9. Mean 200 hPa zonal wind anomaly (m s^{-1}) over composite days event +6 days to event +10 days for the (a) control integration, and (b) the perturbation experiment. The curved line an approximate wave propagation path, the rectangle in (b) indicates the region for the perturbation experiment. (c) Time mean 200 hPa zonal wind (November to April) in the control integration in shaded colours (m s^{-1}) and SPCZ convective event wind anomaly (b) overlaid in grey contours, note the sign has been changed from (b) (2 m s^{-1} contour interval, zero contour omitted, negative contours dashed).